

Silicon Photonic Four-Channel Optical Add-Drop Multiplexer Enabled by Subwavelength Grating Waveguides

Behnam Naghdi and Lawrence R. Chen, Senior Member, IEEE

Department of Electrical and Computer Engineering, McGill University, Montreal, QC H3A 0E9, Canada

Abstract: Wavelength division multiplexing over optical links provides an effective solution for the bandwidth challenge of off-chip and on-chip communications. We demonstrate a compact silicon photonic four-channel optical add-drop multiplexer enabled by subwavelength-grating-based contra-directional couplers. Pass-bands of the device show on-chip insertion losses below 1.8 dB with wide 3 dB bandwidth of ~6.7 nm suitable for coarse wavelength division multiplexing (CWDM) in short-reach optical interconnect applications. Transmission of 10 Gbit/s data stream through different channels of the multiplexer results in negligible power penalties while interferometric crosstalk-induced power penalties are below 2.8 dB.

Index Terms: Silicon photonics, subwavelength structures, add-drop multiplexers, contra-directional couplers.

1. Introduction

Wavelength division multiplexing (WDM) technique effectively enhances the capacity of optical links to address the ever-increasing demand for bandwidth. Coarse WDM (CWDM) uses wider channel spacing and allows for relaxed constraints on the fabrication perfection and thermal control of WDM components for wavelength alignment and control, and therefore, offers a promising solution for the design of low-cost and low-power short reach optical interconnects.

In CWDM networks, optical add-drop multiplexers (OADMs) serve the key role of routing different WDM channels within the network nodes, and their integrated implementation on silicon-on-insulator (SOI) platform is subject to intensive research since silicon photonics provides the possibility of compact, and monolithic integration of optics and electronics on a single, CMOS-compatible chip [1]. Achieving multi-channel OADMs on silicon has been explored through using different structures including arrayed waveguide gratings [2], echelle diffraction gratings [3], cascaded micro-rings [4], cascaded Mach-Zehnder interferometers (MZIs) (with [5] or without incorporating Bragg gratings [6]), and grating-assisted contra-directional couplers (contra-DCs) [7].

In comparison, designs based on grating-assisted contra-DCs provide advantages such as operation over a single spectral range free from closely spaced resonant modes as well as great design flexibility in achieving desired filtering characteristics, e.g., flat-top pass-bands, in a compact footprint. Improving the performance of grating-assisted contra-DCs lies in increasing the optical phase mismatch between the involved eigenmodes of the asymmetric waveguides, and we recently introduced subwavelength grating (SWG)-based contra-DCs whereby the need for two asymmetric waveguides is addressed by placing a subwavelength grating (SWG) waveguide next to a continuous waveguide allowing a wide operation window (over 120 nm) with short coupling length (~200 μm), minor ripples in the pass-bands, and high rejection of undesirable directional coupling (35 dB) [8].

A contra-DC filter with uniform gratings and a fixed gap provides high pass-band/stop-band extinction ratio but at the expense of strong sidelobes that limit the crosstalk performance in CDWM applications [8]. Recently, a high sidelobe suppression of 27 dB was experimentally demonstrated through a gap-apodized SWG-based contra-DC, but the rejection ratio of the through-port was

limited to only ~ 5 dB within its stop-band, which suits the intended application as a two-port bandpass filter, but put limits on its use as a four-port add-drop filter [9].

In our previous work, in favor of the four-port add-drop functionality of the filter, we experimentally explored a stronger power coupling regime through an effectively narrower gap distance, and correspondingly, adjusted coupling length to reach a compromise between sidelobe suppression and stop-band/pass-band extinction [10]. That demonstration promised the use of gap-apodized SWG-based contra-DCs as a four-port building block of multichannel OADMs, and here, we exploit and investigate this potential by cascading four gap-apodized SWG-based contra-DCs to build a four-channel OADM.

The characterization of the OADM shows wide channel spacings of ~ 8.5 nm with ~ 6.7 nm 3 dB bandwidth. We also examine the transmission of 10 Gbit/s NRZ-OOK data stream through different channels of the multiplexer in both cases of drop and add operation and with and without the presence of interferometric and interchannel crosstalk sources and report bit error rate (BER) measurements. The add and drop operations of single channels with no sources of crosstalk have reference BER performance ($\text{BER} = 10^{-9}$) with negligible power penalties compared to the back-to-back configuration. Interchannel crosstalk has negligible impact on BER performance and while interferometric crosstalk induces power penalties, these are typically below 2.8 dB.

2. Design

The layout of the fabricated OADM in SOI platform is illustrated in Fig. 1(a) and consists of four cascaded add-drop filters. Each of the add-drop filters is implemented as a gap-apodized SWG-based contra-DC with the schematic diagram shown in Fig. 1(b). The four channels of this 10-port OADM share a common input and through port but employ their exclusive drop ports and add ports denoted by the distinctive indices of 1 to 4 in Fig 1(a).

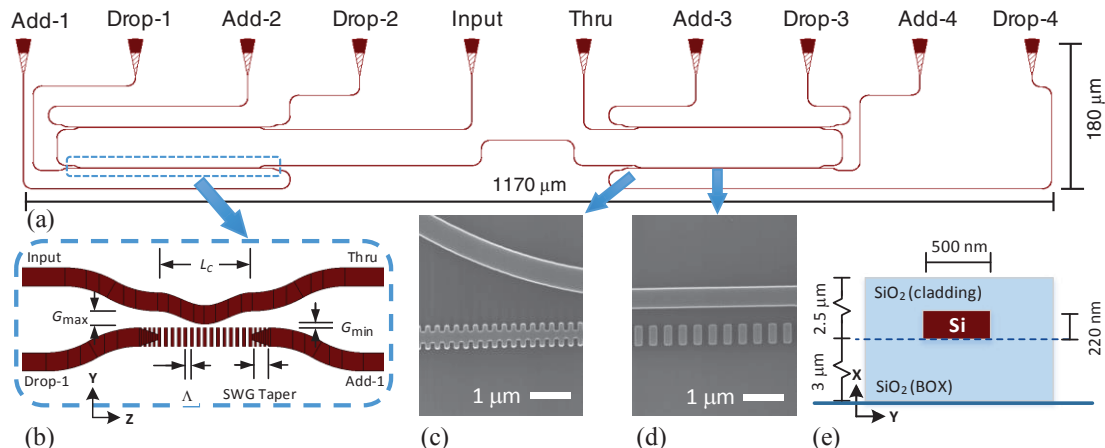


Fig. 1. (a) Layout of the four-channel OADM in SOI platform. (b) Schematic top view of the gap-apodized SWG-based contra-DCs. (c) SEM images of the mode-transition region and (d) coupler region. (e) Cross-section of the strip waveguide.

In all of the four contra-DCs, a strip waveguide is being brought gradually in a gap distance, $G_{\max} = 400$ nm, of an SWG waveguide to form the coupler waist over the coupling length of $L_c = 200$ μm. Along the waist, the gap is tapered by a raised cosine profile described in (1), such that the minimum gap at the center, $z = L_c / 2$, is $G_{\min} = 200$ nm [10].

$$G(z) = G_{\max} - \frac{1}{2}(G_{\max} - G_{\min}) \left[1 - \cos\left(\frac{2\pi z}{L_c}\right) \right]; 0 \leq z \leq L_c \quad (1)$$

The duty cycles of the four SWG waveguides of the four cascaded add-drop filters are all 50% meaning that the length of one silicon segment is half of the period. However, they incorporate different periods, Δ , of 370, 374, 378 and 382 nm. Accordingly, the phase-match condition of contradirectional coupling, as explained in [6], is satisfied at four different wavelengths and leads to add-drop operation in the corresponding four wavelength channels with the specifications in Table 1.

Focusing vertical grating couplers (VGCs) optimized for TE operation are used to couple light into and out of the chip [11]. However, the operation of the device can be extended to both polarizations by employing polarization beam splitting vertical grating couplers that couple the orthogonal fiber modes into the separate waveguides [12]. SWG tapers at the input and output of the SWG waveguides are responsible for adiabatic mode transition and are comprised of silicon blocks that incorporate a fixed period of 250 nm, but a width that varies from 500 nm to 150 nm over a length of 15 μm as schematically shown in Fig. 1(b). The chip area of the four-channel OADM (including the VGCs routing) is 1170 $\mu\text{m} \times 180 \mu\text{m}$ while the footprint of each SWG-based contra-DC is 250 $\mu\text{m} \times 20 \mu\text{m}$. The height and width of all the strip waveguides are 220 nm and 500 nm, respectively, as shown in the cross-section view in Fig. 1(e). The waveguides sit on a 3 μm thick buried oxide (BOX) layer and a 2.5 μm thick cladding of SiO₂ is deposited on top. The devices were fabricated using electron beam lithography, in a single, full, plasma etching process, at the University of Washington Nanofabrication Facility (WNF) [13].

3. Experimental Setup

Fig. 2 shows the diagram of the experimental setup used for characterizing the OADM. An 8-port fiber ribbon array based on polarization maintaining fibers with a fiber to fiber spacing of 127 μm is used to launch the light into and out of the chip, and out of necessity, it has to move to provide access to the appropriate ports of the 10-port OADM (for practical use, a fiber ribbon array with larger port count can be used). For the spectral characterization of the device, the modulators are bypassed and the continuous wave (CW) outputs from the tunable lasers (TLS) are directly launched into the input port and the add ports of the OADM and are monitored at the drop ports and the through port by the optical power meters (PWMs) #1 and #2 to evaluate the drop and add operation of the device, respectively.

On the other hand, for BER characterization, the outputs from the two CW lasers are first modulated by electro-optic Mach-Zehnder modulators (EO-MZMs) driven by separate electrical pulse pattern generators (PPGs) which share the same clock signal but are set to generate uncorrelated bit sequences. The modulated signals are then applied to the input port and/or the add port of the OADM and the output signal is collected from either the drop port or through port of the OADM decided at the indicated switching point in the diagram corresponding to the characterization of either the add or drop operation.

The power of the signal that reaches the receiver of this communication link is controlled by a variable optical attenuator (VOA) and monitored by PWM #3 to enable the characterization of the BER performance versus the received optical power. The polarization controllers (PCs) are used to optimize performance. The receiver comprises an erbium-doped fiber amplifier (EDFA) which is configured to provide a constant output power, a tunable 0.8 nm bandpass filter (BPF) to remove ASE noise, and a photodiode (PD). It should be noted that, for all the experiments, the chip is operated at room temperature without any active temperature stabilization.

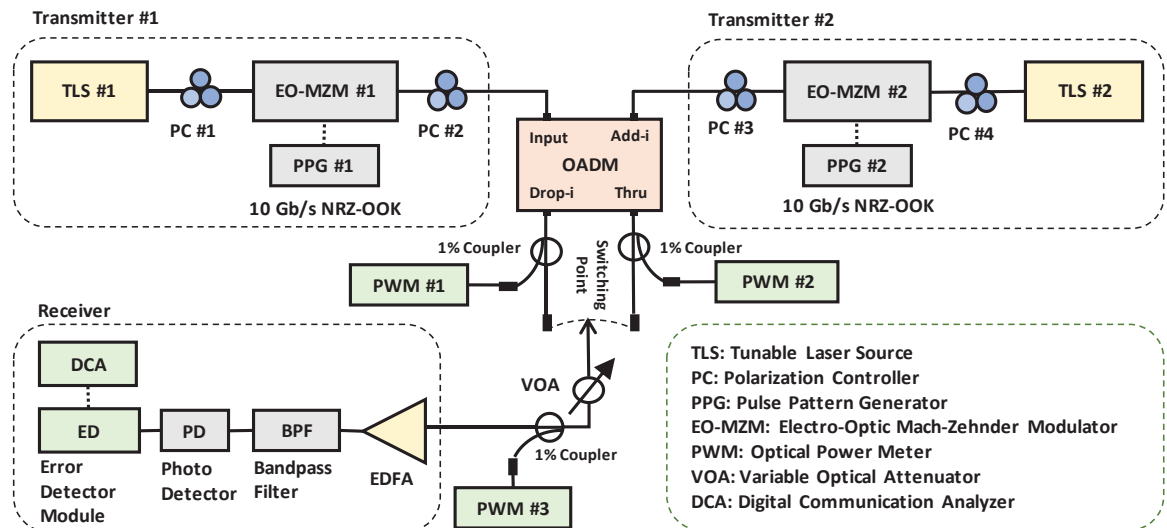


Fig. 2. Diagram of the experimental setup with index $i \in [1, 2, 3, 4]$ denoting the channel under test.

4. Results

4.1 Spectral measurements

Fig. 3(a) demonstrates the spectral responses of the OADM when the light is launched into the input port and the output is monitored at drop ports 1 to 4 individually (corresponding to the drop operation at different channels) as well as at the through port (to observe input-to-through transmission). In Fig. 3(b), the add operation is evaluated by launching light at the different add ports corresponding to channels 1 to 4 and monitoring the output at the through port. All the reported spectra are normalized to the back-to-back insertion loss of a test pair of VGCs with a central loss of ~ 15 dB and a 3 dB bandwidth of ~ 30 nm.

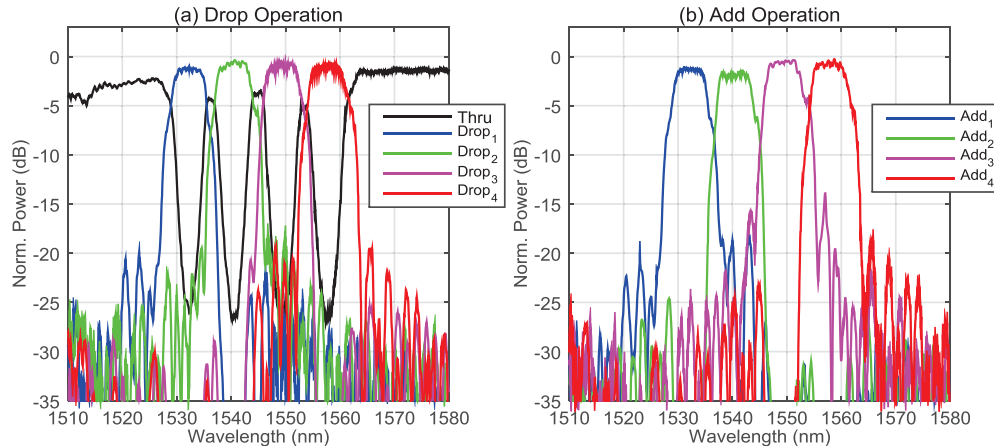


Fig. 3. Measured spectral responses: (a) output at the drop ports and through port when light is launched into the input port and (b) output at the through port when light is launched into the different add ports. The wavelength resolution, which is set by the step size of the tunable laser, is 50 pm.

In agreement with the Lorentz reciprocity theorem, the drop operation responses in Fig. 3(a) are similar to their counterpart add operation responses in Fig. 3(b) within the repeatability of the measurements and the left-right symmetry of the fabricated device. Table 1 summarizes the spectral parameters of the pass-bands of channels 1 to 4 for add and drop operations. The insertion loss of the channels is below 1.8 dB and the input-to-through transmission loss for a signal next to channel 1 or channel 4 is 1.6 dB or 0.8 dB, respectively. The pass-bands of the drop and add responses for the different channels are centered at the wavelengths reported in Table 1 and lead to channel spacings of 8.3, 8.8, and 8.4 nm. The 3 dB bandwidths of the channels are ~ 6.7 nm while the transmission isolation at the center of the channels is ~ 25 dB.

Table 1. Spectral Characteristics
of the Add and Drop Operation of the Four-Channel OADM

Channel Number	Ch-1	Ch-2	Ch-3	Ch-4	
Transmission Isolation (dB)	24.8	25.2	25.1	25.2	
Central Wavelength (nm)	1532.3	1540.6	1549.4	1557.8	
Insertion Loss (dB)	Drop Operation	-1.3	-0.7	-0.9	-1.0
	Add Operation	-1.3	-1.8	-0.6	-0.8
3 dB Bandwidth (nm)	Drop Operation	6.4	6.7	6.7	7.0
	Add Operation	6.4	6.6	6.9	7.0

From Fig. 3(a), the design of the gap apodization and channel spacing has succeeded in reaching a compromise between transmission isolation and crosstalk performance in the sense that the suppression ratios of the spectral sidelobes are in balance with the rejection ratio of the input signal in passing to the through port. In other words, a stronger gap apodization could provide larger suppression of the pass-band sidelobes, but it would be at the expense of weaker coupling regime, and consequently, lower transmission isolation, and vice versa, a diminished apodization profile provides stronger coupling, and accordingly, better transmission isolation, but it would mean stronger pass-band sidelobes and deteriorated crosstalk performance of the multiplexer.

4.1.1 Interferometric crosstalk levels

To evaluate the spectral impact of the interferometric crosstalk on the drop operation, the spectral output at the drop port is compared in the two cases that the CW signal is launched into (1) only the input port and (2) only into the add port. We repeat a similar procedure to evaluate the crosstalk level for the add operation except that the output signal is collected at the through port instead. The two TLLs of the experimental setup are set to provide CW outputs at the same wavelength and with the same power to be launched into the input port or the appropriate add port of the OADM.

Fig. 4 shows spectral results when the CW lasers are tuned to the central wavelengths of the four channels as specified in Table 1. The differences in the peaks of the traces denoted by Δ_{peaks} in Fig. 4 indicate the levels of the interferometric crosstalk at the central wavelengths of the four channels, which ranges from -25.3 dB for the add operation at channel 4 up to -23.4 dB for the drop operation at channel 1. Note that the absolute values of the peaks are evolving in accordance with the wavelength dependent coupling loss of the VGCs.

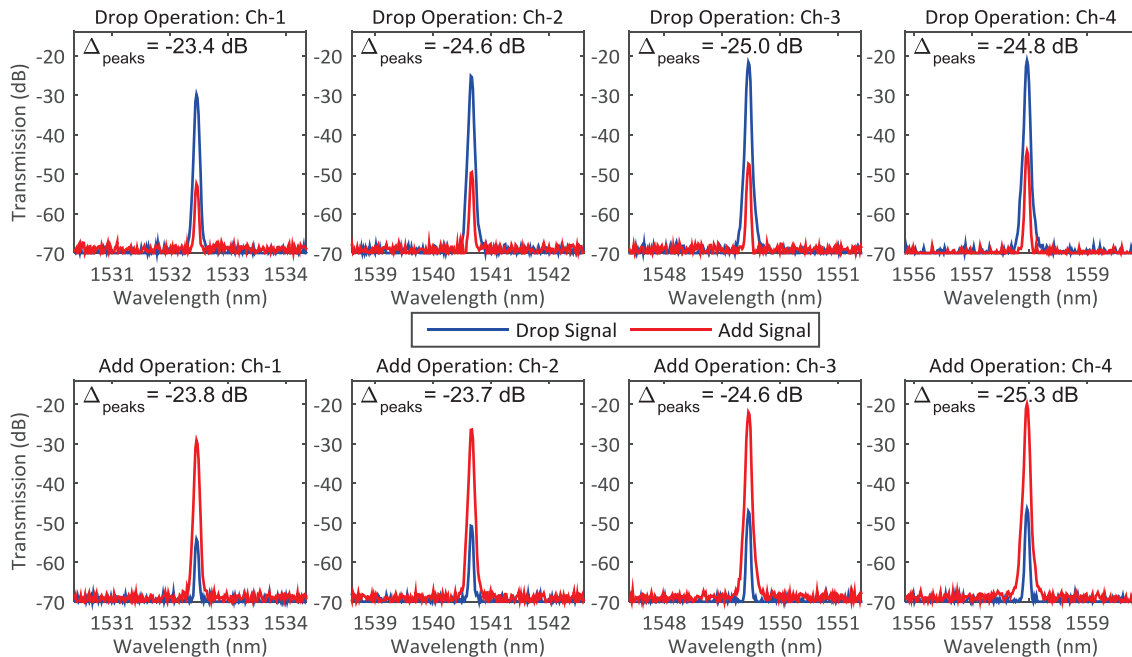


Fig. 4. Spectral measurements on the OSA collected at the drop ports and the through port to study the drop and add operation of the device, respectively, when the CW lasers are tuned to central wavelengths of the four channels. The blue (red) traces represent the drop (add) signals. The differences in the peaks of the plots denoted by Δ_{peaks} indicate the levels of the interferometric crosstalk.

To investigate the case that the OADM channels are not perfectly aligned with the carrier wavelength of the corresponding signals, the two CW lasers are detuned simultaneously and Fig. 5 shows the interferometric crosstalk levels as a function of wavelength detuning from the central wavelengths of the channels normalized to their 3 dB bandwidths. As expected, the traces confirm that the crosstalk levels are stronger for greater values of wavelength detuning. However, a

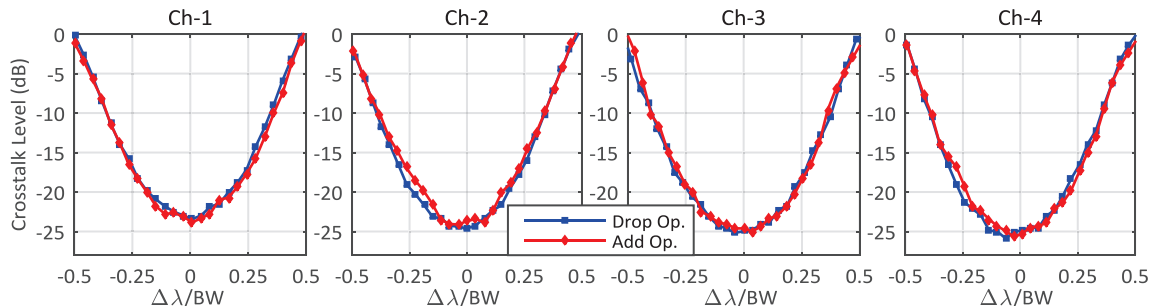


Fig. 5. Interferometric crosstalk levels as a function of normalized wavelength detuning relative to the 3 dB bandwidth of the channels for both drop (blue) and add (red) operation.

detuning less than one quarter of the 3 dB bandwidth allows for interferometric crosstalk levels below -15 dB.

4.1.2 Interchannel crosstalk levels

In the drop port of the m^{th} channel of the OADM, in addition to the desired drop signal centered at λ_m , there is interchannel crosstalk in the form of power leakage from out-of-band add and drop signals centered at $\lambda_n \neq \lambda_m$. Therefore, it is important to study the power leakage of the CW add and drop signals with $\lambda_n \neq \lambda_m$ to the drop port of channel m . Table 2 summarizes the measured crosstalk levels showing that the worst-case crosstalk is -21.6 dB corresponding to the leakage of the drop signal centered at λ_3 to the drop port of channel 2.

Table 2. Interchannel crosstalk levels
at the drop port of channel m due to CW add and drop signals with $\lambda_n \neq \lambda_m$.

Drop Port Index	Ch-1			Ch-2			Ch-3			Ch-4		
Wavelength Index of CW Signal	λ_2	λ_3	λ_4	λ_1	λ_3	λ_4	λ_1	λ_2	λ_4	λ_1	λ_2	λ_3
Crosstalk Level (dB) if CW Drop Signal	-47.3	-31.6	-28.4	-32.9	-21.6	-34.2	-46.3	-48.5	-44.9	-51.2	-49.5	-24.7
Crosstalk Level (dB) if CW Add Signal	-23.0	-43.9	-45.4	-51.6	-59.7	-60.1	-36.5	-28.1	-22.6	*NA	-29.2	-58.1

*The 8-port fiber ribbon array does not provide simultaneous access to the add port of ch-1 and the drop port of ch-4.

4.2 BER measurements

The interference of a transmitted signal with different crosstalk sources is expected to degrade the quality of the received signal and effectively impact a communication link. To evaluate this, we investigate the BER performance in transmission of 10 Gbit/s NRZ-OOK signals with a $2^{31}-1$ pseudo random bit sequence (PRBS) through different channels of the OADM in both cases of add and drop operation and compare it with the case that another independent 10 Gbit/s signal is simultaneously routed by the OADM and acts as a crosstalk source. Moreover, we compare the BER performance to the back-to-back configuration to assess how the non-ideal pass-bands of the OADM degrade the system performance as the pass-bands are not ideally flat and suffer from degrees of phase and magnitude ripples.

First, the transmitters are operated at the central wavelengths of the channels with one being connected to the input port and the other into the add port to obtain the BER curves shown in Fig.

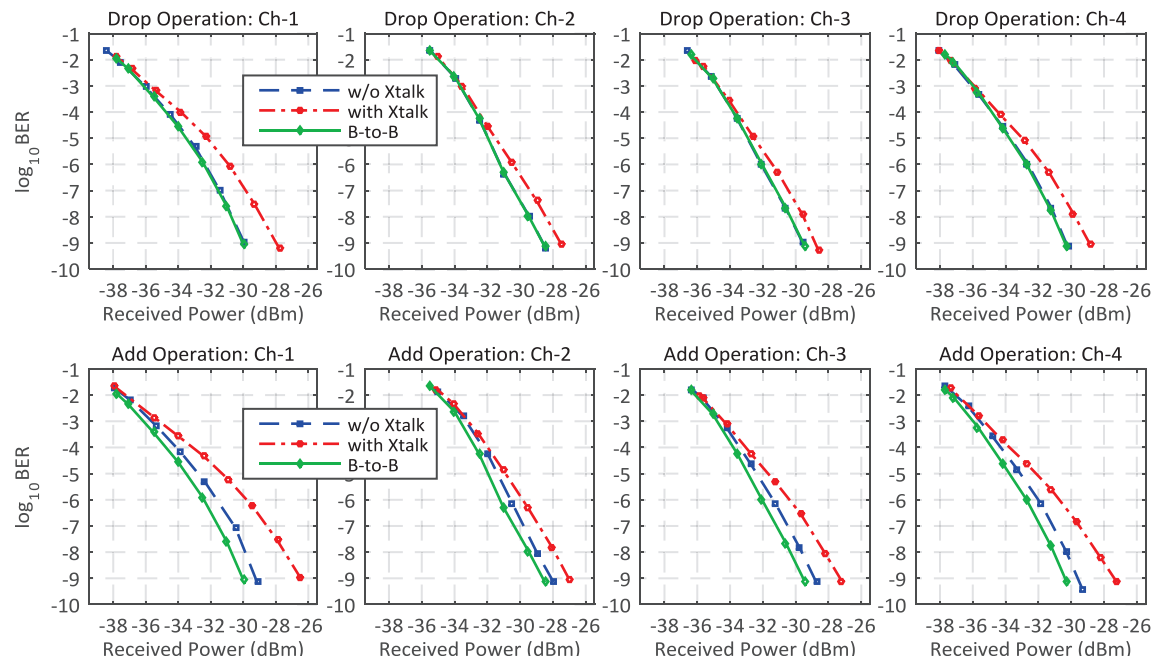


Fig. 6. BER measurements with (dot-dashed red) and without (dashed blue) the interferometric crosstalk compared to the back-to-back case (solid green) for both the drop and add operation while the carrier wavelength of the 10 Gbit/s data is set at the centers of channels 1 to 4.

6. To measure the BER of the drop (add) operation while there is no interfering add (drop) signal, only the transmitter connected to the input port (add port) launches the optical power. In the absence of crosstalk, the drop and add operation of the OADM induce no measurable power penalty and a power penalty of ~ 0.7 dB, respectively, for reference BER performance ($\text{BER}=10^{-9}$) compared to the back-to-back case. For the case of interferometric crosstalk, the BER measurements are obtained by setting the two transmitters to launch simultaneously equal optical power into the input and the add ports of the device. The presence of the interferometric crosstalk induces additional power penalties of < 2.0 and < 2.8 dB for the drop and add operation, respectively.

Second, in Fig. 7, we repeat the preceding BER measurements while the two transmitters operate at the same wavelength that sweeps over the bandwidth of the channels, whereby we study how the interferometric crosstalk-induced power penalties evolve if the OADM channels are not perfectly aligned with the carrier wavelength of the corresponding add and drop signals. In agreement with the variation of crosstalk levels over the bandwidth, the interferometric crosstalk-induced power penalties tend to be higher when the signals are further detuned from the center wavelength of the channels.

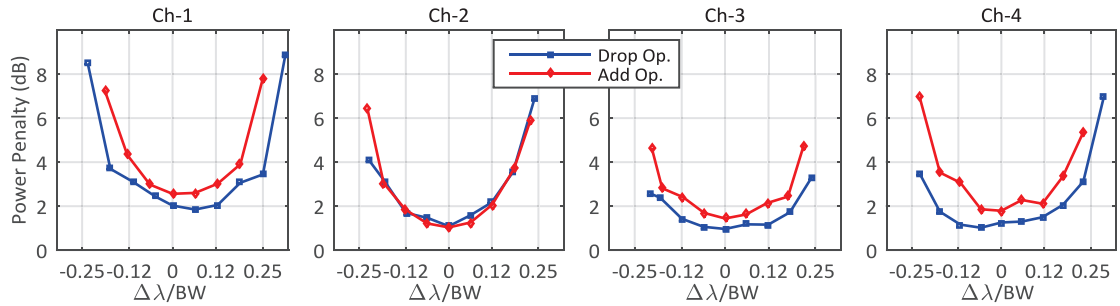


Fig. 7. Interferometric crosstalk-induced power penalties (for $\text{BER} = 10^{-9}$) as a function of normalized wavelength detuning relative to the 3 dB bandwidth of the channels for both drop (blue) and add (red) operation obtained by running the two transmitters at the same wavelength that sweeps over the bandwidth of the channels.

Fig. 8 shows examples of electrical eye diagrams captured at the receiver for the signal corresponding to channel 3. Compared to the back-to-back case, the signal quality is almost unaffected by passing through the OADM as either a drop or add signal. However, by adding interferometric crosstalk, the signal quality slightly degrades in the form of additional intensity noise that leads to partial eye closure.

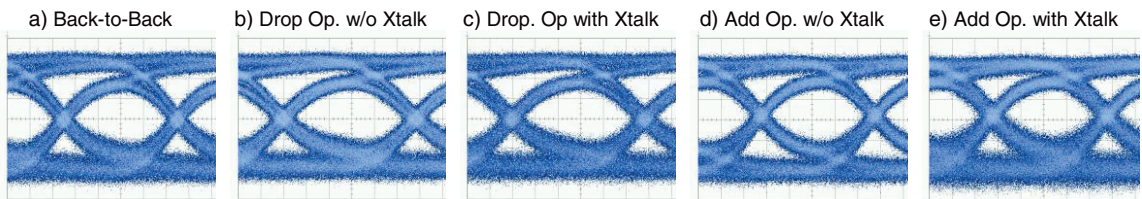


Fig. 8. Measured eye diagrams on the DCA for detected electrical signals corresponding to channel 3 at a fixed received power of -23 dBm in the cases of: a) back-to-back, drop operation b) without or c) with the interferometric crosstalk, and add operation d) without or e) with the interferometric crosstalk.

Next, we evaluate the BER performance in the presence of interchannel crosstalk at the drop ports. From Table 2, the highest interchannel crosstalk level corresponds to -21.6 dB leakage of the drop signal centered at λ_3 to the drop port of channel 2. To evaluate the BER degradation in this case, the two transmitters, one operating at λ_2 (i.e., the desired drop channel) and the second operating at λ_3 (i.e., the crosstalk source), are combined and launched into the input port with equal power while the output signal is received at the drop port of channel 2. In the BER measurements, turning the interchannel crosstalk source on/off showed negligible impact on the BERs, either with or without employing the 0.8 nm BPF on the receiver side. By removing the BPF filter, although the levels of the received interferometric and interchannel crosstalks are comparable, the interchannel crosstalk-induced power penalties are negligible in agreement with the fact that the beat noise arising from the interchannel (out-of-band) crosstalk lies beyond the

bandwidth of the PD, while in the case of interferometric (in-band) crosstalk, the signal-crosstalk beat noise is able to partially lie inside the PD bandwidth and effectively induce power penalty [14, 15].

Lastly, Fig. 9 shows BER measurements for input-to-through transmission of an input signal next to channel 4 with the carrier wavelength of 1566.3 nm. Passing through the OADM results in 0.2 dB power penalty implying that the signal quality is highly preserved compared to an ideal transmission with similar insertion loss.

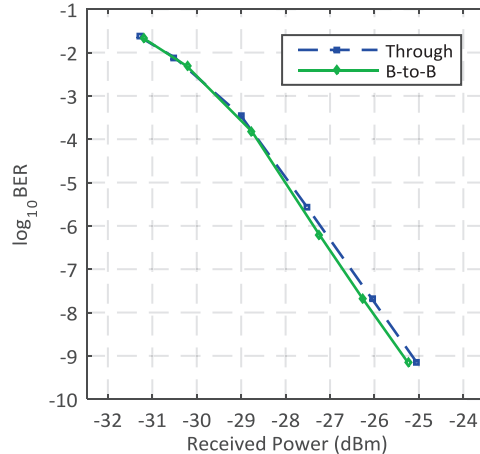


Fig. 9. BER measurements for input-to-through transmission (dashed blue) at $\lambda = 1566.3$ nm compared to the back-to-back case (solid green).

5. Summary

We have demonstrated a new design of multi-channel OADMs based on using SWG-based contra-DCs in SOI. The chip area of the four-channel multiplexer (including the VGCs routing) is $1170 \mu\text{m} \times 180 \mu\text{m}$ while the footprint of each SWG-based contra-DC is $250 \mu\text{m} \times 20 \mu\text{m}$. The characterization of the OADM shows wide channel spacings of ~ 8.5 nm with ~ 6.7 nm 3 dB bandwidth. Insertion loss of the channels is below 1.8 dB with ~ 25 dB transmission isolation at the center of the channels while input-to-through transmission for a signal next to channel 1 or channel 4 is subject to 1.6 dB or 0.8 dB insertion loss, respectively. We also examine the transmission of 10 Gbit/s NRZ-OOK data stream through different channels. The add and drop operations of single channels show reference BER performance with negligible power penalties compared to the back-to-back configuration and adding the interchannel crosstalk has insignificant impact on BER performance. However, the interferometric crosstalk sources are able to induce power penalties below 2.8 dB. Cascading N stages of SWG-based contra-DCs enables the design of N-channel OADMs while the great design flexibility of SWG-based contra-DCs allows for application-specific customization in terms of size, channel bandwidth, transmission isolation, etc. For instance, one might tailor the coupling gap to effectively adjust the channel bandwidth or employ contra-DCs with longer coupling lengths to obtain OADMs with higher transmission isolation at the expense of increased chip size. In this work, we were aimed at the design and characterization of a passive OADM device with wide channel spacing. However, there is the possibility of fine, active tuning of the central wavelengths of the OADM channels, e.g. by implementation of electrically driven metal heaters on top of the contra-DCs. Moreover, for future investigations, a more detailed analysis of the impact of fabrication errors on the performance of the OADM can be carried out.

Acknowledgements

The devices were fabricated by Richard Bojko at the University of Washington Nanofabrication Facility (WNF), a member of the National Science Foundation's National Nanotechnology Infrastructure Network (NNIN). This research was supported in part by Fonds de Recherche du Québec - Nature et Technologies (FRQNT) and Natural Sciences and Engineering Research Council of Canada (NSERC) via CREATE SiEPIC Program.

References

- [1] D. Dai and J. E. Bowers, "Silicon-based on-chip multiplexing technologies and devices for Peta-bit optical interconnects," *Nanophotonics*, vol. 3, no. 4-5, pp. 283-311, 2014.
- [2] J. Zou, Z. Le, J. Hu, and J.-J. He, "Performance improvement for silicon-based arrayed waveguide grating router," *Opt. Express*, vol. 25, no. 9, pp. 9963-9973, 2017.
- [3] S. Pathak, P. Dumon, D. Van Thourhout, and W. Bogaerts, "Comparison of AWGs and echelle gratings for wavelength division multiplexing on silicon-on-insulator," *IEEE Photonics J.*, vol. 6, no. 5, pp. 1-9, 2014.
- [4] P. Chen, S. Chen, X. Guan, Y. Shi, and D. Dai, "High-order microring resonators with bent couplers for a box-like filter response," *Opt. Lett.*, vol. 39, no. 21, pp. 6304-6307, 2014.
- [5] J. Wang and L. R. Chen, "Low crosstalk Bragg grating/Mach-Zehnder interferometer optical add-drop multiplexer in silicon photonics," *Opt. Express*, vol. 23, no. 20, pp. 26450-26459, 2015.
- [6] F. Horst, W. M. Green, S. Assefa, S. M. Shank, Y. A. Vlasov, and B. J. Offrein, "Cascaded Mach-Zehnder wavelength filters in silicon photonics for low loss and flat pass-band WDM (de-) multiplexing," *Opt. Express*, vol. 21, no. 10, pp. 11652-11658, 2013.
- [7] W. Shi, H. Yun, C. Lin, M. Greenberg, X. Wang, Y. Wang, et al., "Ultra-compact, flat-top demultiplexer using anti-reflection contra-directional couplers for CWDM networks on silicon," *Opt. Express*, vol. 21, no. 6, pp. 6733-6738, 2013.
- [8] B. Naghdi and L. R. Chen, "Silicon photonic contradirectional couplers using subwavelength grating waveguides," *Opt. Express*, vol. 24, no. 20, pp. 23429-23438, 2016.
- [9] B. Liu, Y. Zhang, Y. He, X. Jiang, J. Peng, C. Qiu, et al., "Silicon photonic bandpass filter based on apodized subwavelength grating with high suppression ratio and short coupling length," *Opt. Express*, vol. 25, no. 10, pp. 11359-11364, 2017.
- [10] B. Naghdi and L. R. Chen, "Spectral engineering of subwavelength-grating-based contradirectional couplers," *Opt. Express*, vol. 25, no. 21, pp. 25310-25317, 2017.
- [11] Y. Wang, X. Wang, J. Flueckiger, H. Yun, W. Shi, R. Bojko, et al., "Focusing sub-wavelength grating couplers with low back reflections for rapid prototyping of silicon photonic circuits," *Opt. Express*, vol. 22, no. 17, pp. 20652-20662, 2014.
- [12] D. Tailaert, H. Chong, P. I. Borel, L. H. Frandsen, R. M. De La Rue, and R. Baets, "A compact two-dimensional grating coupler used as a polarization splitter," *IEEE Photonics Technol. Lett.*, vol. 15, no. 9, pp. 1249-1251, 2003.
- [13] R. J. Bojko, J. Li, L. He, T. Baehr-Jones, M. Hochberg, and Y. Aida, "Electron beam lithography writing strategies for low loss, high confinement silicon optical waveguides," *J. of Vacuum Sci. & Technol. B*, vol. 29, no. 6, p. 06F309, 2011.
- [14] G. P. Agrawal, *Fiber-optic communication systems*: John Wiley & Sons, 2012.
- [15] H. Takahashi, K. Oda, and H. Toba, "Impact of crosstalk in an arrayed-waveguide multiplexer on NxN optical interconnection," *J. Lightwave Technol.*, vol. 14, no. 6, pp. 1097-1105, 1996.